Dynamics of Spontaneous Vesicle Formation in Dilute Solutions of Amphiphilic Diblock Copolymers

Xuehao He and Friederike Schmid

Fakultät für Physik, Universität Bielefeld,

D-33615 Bielefeld, Germany

ABSTRACT: We study the dynamics of vesicle formation in an initially homogeneous dilute solution of amphiphilic diblock copolymers, using the external potential dynamics (EPD) method. The system was quenched into the unstable two phase region inside the spinodal curve. We discover a new pathway of spontaneous vesicle formation: First, spinodal decomposition sets in and the fluid acquires a weakly modulated structure. After an incubation time, the composition fluctuations of this background pattern trigger the nucleation of spherical micelles. In a third step, copolymers from the solution slowly aggregate to the micelles, they grow and become semivesicles (bigger spherical micelles with a solvent-philic core). Finally, solvent particles diffuse into the semivesicles, and they become full vesicles. We show that the solvent-philic parts of the copolymers play a crucial role for the transition from semivesicles to vesicles. The different contributing mechanisms are discussed and a simple method to control vesicle formation by using uniform sphere micelles as seeds is proposed.

*Corresponding author. E-mail: xhhe@physik.uni-bielefeld.de and schmid@physik.uni-bielefeld.de

1. Introduction

Vesicles, composed of lipid molecules in biology, fulfill important functions for life such as storage and transportation[1]. They can also be formed artificially from amphiphilic block copolymers. This provides the possibility to mimic biological vesicles and has an extraordinary potential in applications such as micro-reactors and nanodevices for encapsulation and controlled release[2-9]. The formation and the stability of vesicles are the focus of intense research[10]. Theoretical studies have shown that vesicles can be stabilized in systems of mixed surfactants, because different surfactant compositions in the outer and inner layers of the vesicle can induce spontaneous curvature[11-14]. However, vesicles can also form spontaneously in single-component solutions of amphiphilic molecules, lipids or amphiphilic block copolymers with narrow length distribution, although such vesicle structures are metastable. How vesicles spontaneously form in such a system, and whether or not the final vesicle structure depends on the dynamics in the system, is not clear till now.

In the past, experimental methods, such as time-resolved dynamic light scattering (DLS), small-angle neutron scattering (SANS) and X-ray scattering (SAXS) have been applied to study, on the millisecond scale, the structural transition from micelles to vesicles, which is induced by mixing two different micellar solutions[15-18]. Transmission electron microscopy (TEM) can provide direct images of aggregative morphologies; however, it is difficult to capture dynamically the fast intermediate structural transitions. Computer simulations provide an important way to peek into this process. Monte Carlo Simulations, Brownian Dynamic, Dissipative Particle Dynamics (DPD) and even Molecular Dynamics with atomistic details have been applied to investigate vesicle formation[19-24]. These studies revealed one possible pathway to vesicle formation (mechanism I): First, small clusters and sphere micelles form; then, the micelles coalesce to small disk micelles (small bilayer structures); finally, the bilayers curve around and close up to form a vesicle. The mechanism relies on the formation of disk micelles, i.e., small bilayer fragment, as intermediate states.

Most of the experiments and simulations focused on studying the vesicle formation in solutions of lipid molecules or small surfactant molecules in water. Compared to these low-molecular weight molecules, amphiphilic block copolymers have much longer chains, with several hundred carbon units in the solvent-phobic block, and up to several tens of units in the solvent-philic block (the hydrophobic tails of lipid molecules are short chains with up to 10-24 carbon units, and the hydrophilic part is only one large molecular group). Another difference is that the molecular interaction per segment is small for polymers, but can be tuned to some extent. The aggregation process is relatively slow due to the slow diffusion of the large molecules, and the weaker segregation. Studying such systems with particle models (MD or DPD) such as the ones mentioned above is computationally very expensive, and large system sizes are necessary to investigate the structures formed by long chain molecules in dilute systems.

Very recently, vesicles of amphiphilic diblock copolymer in dilute solution were obtained using the polymer self-consistent field theory (SCF) method[25]. The SCF theory[26], a mesoscopic polymer theory originally introduced by Edwards[27] in the 1960s and adapted by Helfand and others to treat inhomogeneous polymer systems, has been widely applied to study the performance of polymer blends and block copolymers[25-34]. In field theory, the particles (atoms or coarse-grained beads) in the system are converted into the conjugated potential fields, and the computing cost only depends on the sample size. Furthermore, field theory is built on the framework of a local free energy and thus favorable to the analysis of thermostability. In Ref. 25, the SCF approach was applied to the study of vesicle formation in 2 dimensions (2D) using a "pseudodynamic" method and various vesicle structures were discovered. The simulation demonstrated that the final vesicle structure strongly depends on the dynamic aggregation process, as triggered by various initial fluctuations. Uneyama and Doi [35] studied the vesicle structure in 3D using a free energy density functional method and obtained the same results. However, these two calculation schemes did not satisfy the local monomer conservation, and thus did not mimic to a real dynamical process. More realistic simulations are required to gain deeper insight into the dynamic process of vesicle formation.

Sevink and Zvelindovsky[36] studied the self-assembly of complex vesicles of short surfactant ($A_2B_n, 2 \le n \le 6$) using the dynamic self-consistent field theory (DDFT). They report on a mechanism of vesicle formation which is similar to the conventional one (Mechanism I mentioned above).

In this paper, external potential dynamics (EPD)[37-41] was applied to study the spontaneous formation of vesicles of amphiphilic diblock copolymers in dilute solution. In EPD, the monomer concentration is a conserved quantity, and the polymer dynamics is inherently of Rouse type. We report on a new pathway of spontaneous vesicle formation which differs from the conventional one (Mechanism I). The process of spontaneous vesicle formation is described in detail. The origin of the new mechanism and possible applications based on this mechanism are discussed.

2. External potential dynamics based on dynamic self-consistent field theory

We consider a mixture of amphiphilic diblock copolymers P, and solvent particles S in a system of volume V. Every copolymer chain has two parts, a solvent-phobic block A and solvent-philic block B. The volume fractions of segments A and B in the system are f_A and f_B, and the volume fractions of copolymers and solvent in the solution are $f_P = f_A + f_B$ and $f_S = 1 - f_P$, respectively. In the SCF theory, one considers the statistics of a copolymer chain subject to a set of effective chemical potential fields, ω_I, where the index I represents the block species A or B. These chemical potential fields, which replace the actual interactions between different components, are conjugated to the segment density fields ϕ_I of block species *I*. Similarly, solvent molecules are considered to be exposed to an effective chemical potential field ω_S that is conjugate to the solvent density field ϕ_S. The partition function of a solvent particle in the field ω_S is $Q_S = \int dr \exp(-\omega_S)$, and the partition function of a single diblock copolymer chain in the fields ω_A and ω_B is $Q_P = \int dr g(r,1)$, where the end-segment distribution function $g(r,s)$ gives the probability that a section of a chain, of contour length *s* and containing a free chain end, has its

"connected end" located at *r*. The parameterization is chosen such that the contour variable *s* increases continuously from 0 to 1 from one end of the chain to the other. We use a flexible Gaussian chain model to describe the single-chain statistics, thus the function $g(r,s)$ satisfies a modified diffusion equation

$$\frac{\partial}{\partial s} g(r,s) = \nabla^2 g(r,s) - N\omega g(r.s) . \tag{1}$$

This equation satisfies the initial condition, $g(r,0) = 1$. Here ω is ω_A when $0 < s < c_A$ and ω_B when $c_A < s < 1$. Similarly, a second distribution function $g'(r,s)$ (containing the other chain end) also satisfies Eq. (1) with the initial condition $g'(r,0) = 1$, but ω is ω_B when $0 < s < c_B$ and ω_A when $c_B < s < 1$ (c_A and c_B are the length fractions of A and B segments in a diblock copolymer chain and $c_B + c_A = 1$). The density of the monomer components is obtained by evaluating

$$\begin{aligned} \phi_A(r) &= \frac{Vf_P}{Q_P}\int_0^{1-c_B} dsg(r,s)g'(r,1-s) \\ \phi_B(r) &= \frac{Vf_P}{Q_P}\int_{1-c_B}^{1} dsg(r,s)g'(r,1-s) \\ \phi_S(r) &= \frac{Vf_S \exp(-\omega_S(r))}{Q_S} \end{aligned} . \tag{2}$$

Finally, the free energy function per volume (in units of $k_B T$) of the system is

$$\begin{aligned} F/V = &-f_S \ln(Q_S/Vf_S) - \frac{f_P}{N}\ln(Q_P N/Vf_P) \\ &+ \frac{1}{V}\int dr[\chi_{AB}\phi_A\phi_B + \chi_{AS}\phi_A\phi_S + \chi_{BS}\phi_B\phi_S \\ &- \omega_A\phi_A - \omega_B\phi_B - \omega_S\phi_S + \frac{\kappa_H}{2}(\phi_A + \phi_B + \phi_S - 1)^2] \end{aligned} , \tag{3}$$

where *N* is the length of copolymer chain in coarse-grained units (every unit corresponds to several tens monomers), χ_{IJ} is the Flory-Huggins interaction parameters between species i and j that describes the molecular interaction, and κ_H is the coefficient of compression energy. The SCF theory accounts for the linear structure of long chain polymers, and its free energy contains entropic

and energetic contributions from every component. Detailed derivations of the free energy in the SCF theory can be found in the literature, e.g., the review articles Refs. 26 and 34.

To study a realistic dynamical process, we use the external potential dynamics method as originally introduced by Maurits and Fraaije[37]. It is based on the continuity equations for the conserved densities ϕ_I together with an expression for the density currents which is approximately valid for Rouse-type chain dynamics,

$$\frac{\partial \phi_I(r)}{\partial t} = -\nabla_r J_I(r) \qquad \text{with} \qquad J_I(r) = -D\sum_J \int_V dr' P_{IJ}(r,r')\nabla_{r'}\left(\frac{\delta F}{\delta \phi_J} + \eta_J\right). \tag{4}$$

Here, P_{IJ} are two-body correlators introduced in Refs. 37 and 38, and η_J is a Gaussian distributed random noise term that accounts for thermal fluctuations and fulfills

$$\begin{aligned} \langle \eta_I(r,t) \rangle &= 0, \\ \langle \eta_I(r,t)\eta_J(r',t') \rangle &= \beta \delta_{IJ}\delta(t-t')\delta(r-r'). \end{aligned} \tag{5}$$

The dynamical equations (4) can be simplified considerably by reformulating them in terms of the potential field ω_I. Exploiting the relation $P_{IJ}(r,r') = -\delta\phi_I(r)/\delta\omega_J(r')$, one obtains the external potential dynamics (EPD) equations[37]

$$\frac{\partial \omega_I(r)}{\partial t} = -D_I \nabla^2 \left(\frac{\delta F}{\delta \phi_I} + \eta_I\right) \quad , \tag{6}$$

where D_I is a constant diffusion coefficient which depends on the particle type (polymer or solvent). The functional derivative $\delta F / \delta \phi_I$ can be calculated from Eq. (3), giving

$$\begin{aligned} \frac{\delta F}{\delta \phi_{\mathrm{A}}} &= \chi_{\mathrm{AB}}\phi_{\mathrm{B}} + \chi_{\mathrm{AS}}\phi_S + \kappa_{\mathrm{H}}(\phi_{\mathrm{A}} + \phi_{\mathrm{B}} + \phi_{\mathrm{S}} - 1) - \omega_{\mathrm{A}}, \\ \frac{\delta F}{\delta \phi_{\mathrm{B}}} &= \chi_{\mathrm{AB}}\phi_{\mathrm{A}} + \chi_{\mathrm{BS}}\phi_S + \kappa_{\mathrm{H}}(\phi_{\mathrm{A}} + \phi_{\mathrm{B}} + \phi_{\mathrm{S}} - 1) - \omega_{\mathrm{B}}, \\ \frac{\delta F}{\delta \phi_{\mathrm{S}}} &= \chi_{\mathrm{AS}}\phi_{\mathrm{A}} + \chi_{\mathrm{BS}}\phi_B + \kappa_{\mathrm{H}}(\phi_{\mathrm{A}} + \phi_{\mathrm{B}} + \phi_{\mathrm{S}} - 1) - \omega_{\mathrm{S}}. \end{aligned} \tag{7}$$

The set of equations (1), (2), (6) is conveniently solved by simple time iteration methods. We note that hydrodynamic effects are not introduced in this version of EPD. The EPD model has been

applied to study dynamic phase separation in polymer blends and gave much better agreement with Monte Carlo simulation results than a comparable local coupling model[39, 40,41] .

3. Simulation parameters and numerical methods

Our simulation starts from a homogenous initial state with initial external potential fields $\omega_{\mathrm{A}}^{0} = \chi_{\mathrm{AB}} f_{\mathrm{A}} f_{\mathrm{B}} + \chi_{\mathrm{AS}} f_{\mathrm{A}} f_{\mathrm{S}}$, $\omega_{\mathrm{B}}^{0} = \chi_{\mathrm{AB}} f_{\mathrm{A}} f_{\mathrm{B}} + \chi_{\mathrm{BS}} f_{\mathrm{B}} f_{\mathrm{S}}$, and $\omega_{\mathrm{S}}^{0} = \chi_{\mathrm{AS}} f_{\mathrm{A}} f_{\mathrm{S}} + \chi_{\mathrm{BS}} f_{\mathrm{B}} f_{\mathrm{S}}$. Based on the experience in the past[25] , the parameters in the simulation were selected as follows: The chain length was $N = 17$, and the diffusion coefficients were $D_{\mathrm{A}} = D_{\mathrm{B}} = D_{\mathrm{S}} / 17$; the length fraction of the solvent-philic B block, $c_{\mathrm{B}} = 0.118$, was same in all simulations; the polymer concentration in solution was chosen rather small, $f_{\mathrm{P}} = 0.1$; The Flory-Huggins interaction parameter χ_{BS} was varied from -0.15 to 0.75, while $\chi_{\mathrm{AS}} = 1.2$ and $\chi_{\mathrm{AB}} = 1.05$ were kept constant. These parameters correspond to quenching points in the unstable region within the spinodal curve (Fig. 1). The compressibility coefficient was chosen $\kappa_{H} = 1.176$, and the coefficient of thermal noise $\beta = 3.46 \times 10^{-3}$. The numerical simulations were carried out in 2 and 3 dimensions (220×220 square lattice in 2D and $46 \times 46 \times 46$ in 3D, respectively), with grid size $\Delta x / R_{g} = 1/3$ (R_{g} is the unperturbed mean square radius-of-gyration of a copolymer chain), and time step $\Delta t\, D_{S} = 0.51$. The external potentials and density profiles were stored for analysis every 1.0×10^{4} time steps after the quench. The structure factor at the initial stage of phase separation was calculated applying 10 parallel samples. The structure factor is defined as:

$$S(q,t) = < \int_{V} dr_{i} \int_{V_{j}} dr_{j} \exp(iq \cdot r_{ij}) ((\phi_{\mathrm{P}}(r_{i}) - \phi_{\mathrm{S}}(r_{i}))(\phi_{\mathrm{P}}(r_{j}) - \phi_{\mathrm{S}}(r_{j})) - (f_{\mathrm{P}} - f_{\mathrm{S}})^{2}) > \qquad (8)$$

Eq 1 was solved with an improved pseudo spectral method[42], which has higher stability and accuracy than other methods for the same spatial discretization: The diffusion equation (1) was discretized according to

$$g(r,s+ds) = \exp\left[-\frac{ds}{2}N\omega(r)\right]\exp\left[ds\nabla^2\right]\exp\left[-\frac{ds}{2}N\omega(r)\right]g(r,s), \quad (9)$$

and a Fast Fourier Transformation (FFTW) package[43] was applied in the evaluation of the diffusion operator in Eqs. (6) and (9) to ensure precision and convergence.

4. Results and Discussion

Our simulations started from a homogeneous state, which corresponds, in reality, to a quenching process. The quenching points were chosen in the unstable region of the hypothetical *homogeneous* mean-field phase diagram (Fig. 1). The latter was calculated in the Flory-Huggins approximation, i.e., the mixing free energy was expressed as

$$F_{\text{F-H}} = \frac{\phi_{\text{P}}}{N}\text{In}(\phi_{\text{P}}) + \phi_{\text{S}}\text{In}(\phi_{\text{S}}) + \chi_{\text{AB}}\phi_{\text{A}}\phi_{\text{B}} + \chi_{\text{AS}}\phi_{\text{A}}\phi_{\text{S}} + \chi_{\text{BS}}\phi_{\text{B}}\phi_{\text{S}}. \quad (10)$$

Inserting $\phi_{\text{A}} = c_{\text{A}}\phi_{\text{P}}, \phi_{\text{B}} = c_{\text{B}}\phi_{\text{P}}$ and $\phi_{\text{S}} = 1-\phi_{\text{P}}$, we obtained

$$F_{\text{F-H}} = \frac{\phi_{\text{P}}}{N}\text{In}(\phi_{\text{P}}) + (1-\phi_{\text{P}})\text{In}(1-\phi_{\text{P}}) + \chi_{\text{AB}}c_{\text{A}}c_{\text{B}}\phi_{\text{P}}^{\ 2} + (\chi_{\text{AS}}c_{\text{A}} + \chi_{\text{BS}}c_{\text{B}})(1-\phi_{\text{P}})\phi_{\text{P}}. \quad (11)$$

The limit of thermodynamic stability or spinodal corresponds to the points of the inflection, $\partial^2 F_{\text{F-H}} / \partial^2 \phi_{\text{P}} = 0$. In the case of constant χ_{AS} and χ_{AB}, the spinodal line can be expressed as

$$\chi_{\text{BS}}^{\ spinodal} = \frac{1}{2Nc_{\text{B}}\phi_{\text{P}}} + \frac{1}{2c_{\text{B}}(1-\phi_{\text{P}})} + \chi_{\text{AB}}c_{\text{A}} - \chi_{\text{AS}}\frac{c_{\text{A}}}{c_{\text{B}}}. \quad (12)$$

For $\phi_{\text{P}} = 0.1, \chi_{\text{AS}} = 1.2, \chi_{\text{AB}} = 1.05$, $\chi_{\text{BS}}^{\ spinodal}$ equals -0.85. Our simulation points were located in the unstable region close to the spinodal line (Fig. 1, χ_{BS} ranges from -0.15 to 0.75). We note that the full mean-field phase diagram, which has not been calculated, also contains microphase separated regions.

The dynamic simulations in 2D and 3D showed that vesicles can form spontaneously from the homogeneous state. Figs. 2 and 3 show the evolution process of vesicle formation for the case of $\chi_{\text{BS}} = 0.0375, \chi_{\text{AS}} = 1.2, \chi_{\text{AB}} = 1.05$ in 2D and 3D. First, after an initial period of aggregation

(which we identified as spinodal decomposition as discussed in detail below), stable copolymer droplets appear rather suddenly after about 3.3×10^5 time steps in 2D (Fig. 2), and 4.1×10^5 steps in 3D (Fig. 3). After that, the droplets grow larger and larger, and rearrange to form spherical micelles. After 3.6×10^5 time steps in 2D and 4.5×10^5 time steps in 3D, a B-rich region appears in the center of the sphere. Finally, solvent diffuses inside and a hollow body, i.e., a vesicle, is formed.

The initial stage displays the typical features of spinodal decomposition. This is easily explained by the fact that the initially disordered system is quenched into the unstable part of the homogeneous two phase region. As predicted by the Cahn-Hilliard theory[44], the early-stage demixing is governed by the growth of unstable fluctuations with definite nonzero wavelength, which leads to the formation of a complex interconnected modulated structure (Fig. 4). More detailed information can be gained from the inspection of the structure factor $S(q,t)$ (Eq. (8)) at different times (Fig. 5). As expected, $S(q,t)$ features a peak at a well-defined wave vector $q_{\max}$. According to the linearized Cahn-Hilliard theory, the position of the peak should not change with time; however, it has long been known theoretically[45,46] and was also confirmed experimentally[47], that this particular result of the linearized theory is never valid: $q_{\max}$ gradually shifts to lower values already in the earliest stages of spinodal decomposition. This is also observed in our simulations (Fig. 5, bottom): At very early times, a peak first emerges in $S(q,t)$ and then immediately starts moving to lower q values. Soon, however, the peak position settles at $q_{\max}R_g \approx 1.7$ and does not change any more (Fig. 5, middle). We attribute that to the amphiphilic structure of the copolymers, which introduce an intrinsic wavelength of the order R_g in the copolymer-rich phase. A similar behavior has been predicted generally for spinodal phase separation into two fluids, of which one is structured [48].

After some time, the composition fluctuations become strong enough that they are able to trigger the sudden formation of stable copolymer droplets. A second stage is entered, which is qualitatively

very different from the first stage: Whereas spinodal decomposition is essentially homogeneous, the subsequent aggregation of copolymers into droplets is a highly inhomogeneous and stochastic process, with similarity to nucleation. Fig. 6 shows the order parameter, defined as $\sigma = \int_V dr\left|\phi_{\mathrm{A}} + \phi_{\mathrm{B}} - f_{\mathrm{P}}\right| / V$, as a function of time for different χ_{BS}. The emergence of droplets is reflected by a sharp increase of the order parameter. We note that the nucleation process in our system is rather different from classical nucleation: The nucleation events take place on the background of the modulated structure generated by the spinodal decomposition. They are not mediated by thermal fluctuations, but by the composition fluctuations of this underlying pattern. As a result, most nucleation events take place at almost the same time, and the order parameter in Fig. 6 very quickly reaches a plateau.

Fig. 6 also illustrates the role of the interaction parameter. Since we have $\chi_{BS} < \chi_{AS}$, the solvent-philic copolymer block slows down the copolymer aggregation (the aggregation is controlled by the parameter $\chi_{\mathrm{AS}}\phi_{\mathrm{P}}\phi_{\mathrm{S}} + (\chi_{\mathrm{BS}} - \chi_{\mathrm{AS}})\phi_{\mathrm{B}}\phi_{\mathrm{S}} + \chi_{\mathrm{AB}}\phi_{\mathrm{A}}\phi_{\mathrm{B}}$), and the aggregation rate decreases with increasing solvent-philicity or decreasing χ_{BS}. This is observed in the spinodal stage (Fig. 6, inset), as well as in the droplet stage. The weaker the solvent-philicity of B segment, the earlier the droplets form, and the higher the number of stable droplets. Simulations in 3D showed the same trend. For the case $\chi_{BS} = -0.45$, stable nuclei formed at 1.17×10^{6} time steps (Fig. 7), while for $\chi_{\mathrm{BS}} = 0.0375$, the first stable nucleus appeared much earlier already after 4.1×10^{5} time steps (Fig. 3).

To analyze these observations on a more quantitative level, we first note that decreasing χ_{BS} moves the quenching point closer to the spinodal (see Fig. 1). This affects the wavelength $\lambda^{*} = 2\pi / q_{\max}$ of the spinodal decomposition pattern as well as the growth rate $1/t^{*}$ of the corresponding composition fluctuations. The behavior of λ^{*} and t^{*} as a function of $(\chi - \chi_{spinodal})$ can be estimated within the Cahn-Hilliard theory[44,48]. The calculation is

straightforward and shall be skipped here. We obtain $\lambda^* \propto (\chi - \chi_{spinodal})^{-1/2}$ and $t^* \propto (\chi - \chi_{spinodal})^{-1}$. The quantities λ^* and t^* set the natural length and time scale in the system at the initial stage. We will now hypothesize that they also determine the density of droplets n_s and the incubation time τ for the droplet formation. This leads to the scaling prediction $n_s \propto (\chi - \chi_{spinodal})^{d/2}$ for the density of stable droplets (*d* is the number of spatial dimensions), and $\tau \propto (\chi - \chi_{spinodal})^{-1}$ for the incubation time. Fig. 8 shows that the simulation data (2D) are consistent with such a scaling behavior. Both n_s and τ can be fitted very well with a power law $(\chi - \chi_{spinodal})^{\alpha}$, and the fit values of α are close to the expected values ($\alpha = 1$ for n_s and $\alpha = -1$ for τ). The slight deviations from 1 may be related to the fact that the Cahn-Hilliard theory is a mean-field theory and only valid at time zero.

After the nucleation of the droplets, copolymers aggregate to them from solution, they grow, and the A and B segments start to rearrange themselves within the droplet under the driving force of the repulsion $\chi_{AB}\phi_A\phi_B$. This is illustrated by the density profiles in Fig. 9. First, the originally disordered droplet microphase separates into a spherical micelle structure with an A-rich core and a B-rich corona. Then, as the micelle continues to grow, its radius eventually exceeds the gyration radius R_g of a chain, a part of the copolymers flip-flop, and B segments enter the center of the micelle (Fig. 9, thick dot-dashed line corresponding to 3.5×10^5 time steps). We call this intermediate structure a semivesicle. Finally, when the radius of the semivesicle exceeds $2R_g$, solvent diffuses inside and the semivesicle turns into a full vesicle (Fig. 9, thick dot-dot-dashed and thick dashed lines corresponding to 4.0×10^5 and 6.0×10^5 time steps). At the same time, a new broad peak appears in the structure function S(*q*, *t*), which gradually moves to smaller *q* values (Fig. 5 top, marked with S). In the following, the vesicle grows further, but much more slowly than before.

The last observation can be rationalized with the following consideration: Like in classical nucleation, the initial growth of the copolymer clusters is driven by the competition of two factors: The bulk chemical energy gained by the aggregation of copolymers from solution (in particular, the energy gain of their A-blocks), and the surface tension. The latter is positive or close to zero, and scales roughly like R^{D-1} for a cluster of size R in D dimensions. The former is negative and initially scales like R^D (for disordered droplets and micelles), but the scaling then crosses over to R^{D-1} (for vesicles). The amplitude of the bulk term decreases with time, since the concentration of copolymers that are still in solution decreases. Hence it can be neglected at late times, if the surface tension is positive. We emphasize that this is radically different from classical droplet nucleation, where the bulk energy scales like R^D for all droplet sizes and thus always dominates for large enough R. In our case, the late-stage growth strongly depends the value of the surface tension: If it is positive, the growth stops. If it is close to zero, the growth may continue.

Consequently, the solvent-philicity of the B-block not only influences the speed of the copolymer aggregation in the initial stage, it also drives the transformation process from semivesicle to vesicle. Fig. 10 shows three examples of late stage configurations for different values of χ_{SB}. If the B-segments are highly solvent-philic, the solvent swells the B-blocks, and free energy can be gained if the solvent enters the semivesicle in order to swell the inner B-rich region. In that case, the surface tension between the swollen B-brushes at the surfaces of the vesicle and the solvent is close to zero, and vesicles form. At low solvent-philicity (i.e., high χ_{SB}), the solvent fails to swell the B-blocks of the polymer, and the surface tension becomes positive. The system then attempts to minimize the total interface between B-rich region and solvent, and semivesicles become more favorable than vesicles. The transition between the semivesicle and the vesicle regime occurs at $\chi_{SB} \approx 0.4$. This value is reasonably close to $\chi_{SB} = 1/2$, which corresponds to the θ-point of B-polymers in solution[49]. The fact that it is slightly lower than $\chi_{SB} = 1/2$ can presumably be

attributed to the confinement of the B-blocks in a brush, which hinders swelling, compared to a dilute solution.

We note that even at vanishing surface tension, the micelles and semi-vesicles are still round. This is because the surface tension of the micelle is mainly determined by the structure of the interfacial region between B-corona and solvent, whereas the shape of the micelle adjusts such that the interfacial area between segregated A- and B-rich regions (the region of A-B contacts) is minimized.

In some of the simulations, we have observed a phenomenon somewhat reminiscent of Ostwald ripening[50-52]: Smaller semivesicles or micelles sometimes started to shrink and released copolymers into the solution (two examples are shown in Fig. 11), which then diffused away to join nearby clusters. Thus larger clusters grew at the expense of the shrinking clusters. The factors which promote this behavior are low solvent-philicity of B and the presence of one or several clusters in close vicinity. However, such shrinking events were never observed for vesicles. We recall that according to the classical Lifshitz-Slyozov theory[50,51], Oswald ripening is driven by the same competition between surface tension and bulk free energy as droplet nucleation. (The surface tension which small droplets to shrink, and the bulk free energy causes large droplets to grow). As discussed above, there is no such competition for hollow vesicles. This explains why full vesicles always remained stable.

Figure 12 shows as a function of time the integrated free energy function F (3), the mixing energies $E_{\mathrm{A}}, E_{\mathrm{B}}$ and E_{S}, and the entropies SS_{P}, and SS_{S}, for the case $\chi_{\mathrm{BS}} = 0.0375$, $\chi_{\mathrm{AS}} = 1.2$, and $\chi_{\mathrm{AB}} = 1.05$. They are defined as follows

$$
\begin{aligned}
E_{\mathrm{A}} &= \int_V dr(\chi_{\mathrm{AB}}\phi_{\mathrm{A}}\phi_{\mathrm{B}} + \chi_{\mathrm{AS}}\phi_{\mathrm{A}}\phi_{\mathrm{S}})/V \\
E_{\mathrm{B}} &= \int_V dr(\chi_{\mathrm{AB}}\phi_{\mathrm{A}}\phi_{\mathrm{B}} + \chi_{\mathrm{BS}}\phi_{\mathrm{B}}\phi_{\mathrm{S}})/V \\
E_{\mathrm{S}} &= \int_V dr(\chi_{\mathrm{AS}}\phi_{\mathrm{A}}\phi_{\mathrm{S}} + \chi_{\mathrm{BS}}\phi_{\mathrm{B}}\phi_{\mathrm{S}})/V \\
SS_{\mathrm{P}} &= f_{\mathrm{P}}\ln(Q_{\mathrm{P}}N/Vf_{\mathrm{P}})/N + \int_V dr(\omega_{\mathrm{A}}\phi_{\mathrm{A}} + \omega_{\mathrm{B}}\phi_{\mathrm{B}})/V \\
SS_{\mathrm{S}} &= f_{\mathrm{S}}\ln(Q_{\mathrm{S}}/Vf_{\mathrm{S}}) + \int_V dr(\omega_{\mathrm{S}}\phi_{\mathrm{S}})/V \\
SS_{\mathrm{P+S}} &= SS_{\mathrm{P}} + SS_{\mathrm{S}}
\end{aligned}
\tag{13}
$$

At the beginning (before 3.0×10^5 time steps), one observes a smooth plateau, corresponding to the stage of spinodal decomposition. The enlarged inset in Fig. 12, top, shows the small fluctuations of the free energy at that stage. After 3.3×10^5 time steps, the free energy decreases sharply (Fig. 12, top), signaling that stable nuclei are formed. Subsequently, more copolymers aggregate to the nucleus, which results in the decrease of E_{A} and E_{S}. In contrast, E_{B} increases due to the increase of contacts between A and B upon copolymer aggregation (Fig. 12, middle). The increase of E_{B} promotes the rearrangement into a spherical micelle with a B-rich corona, and also the transformation from a spherical micelle to a semivesicle. During the aggregation process, the entropy of the system decreases, and its changes mainly comes from the contribution of the solvent (Fig. 12, bottom).

5. Discussion and Summary

We have seen that the spontaneous vesicle formation depends on two synergistic processes, the aggregation of amphiphilic molecules (on the larger scale), and the rearrangement of solvent-phobic and solvent-philic copolymer parts (on the smaller scale). The two processes depend on the chain length and the molecular interactions. For lipid molecules or short surfactants in water solution, the chain length is small and the interaction energies are high, hence the aggregation of molecules and the rearrangement of hydrophilic and hydrophobic parts are fast, and the system quickly reaches local equilibrium, i.e., clusters and small micelles. Most amphiphilic molecules in solution are consumed directly at the initial stage. The later stage is controlled by coalescence and interfacial energy minimization of micelles. In such systems, spontaneous vesicle formation follows the

pathway I described in the introduction: First, clusters and small micelles aggregate, then disk micelles (bilayer fragments) are formed as intermediate structures through the coalescence of micelles, and finally, the bilayer fragments curve and close up to build small vesicles in order to minimize the edge energy.

In contrast, for long amphiphilic diblock copolymer in dilute solution with weak interaction parameters, the aggregation and the rearrangement process are slow, since the diffusion is slow, and the chain relaxation times are long. In such a system, the segregation of A and B segments initially lags behind the aggregation of copolymer, due to the fact that the former depends on local concentration, which is controlled by the latter. We have demonstrated that, at the initial stage, stable droplets appeared while A and B segments were still mixed. Second, A and B segments segregate only weakly. Therefore, the interfacial barrier created by the B-segments, which prevents the remaining copolymers in solution from aggregation, is weak. This facilitates the growth of micelles and further promotes the flip-flop of copolymers, when the size of micelle exceeds the critical value (~2Rg). So, the weak segregation results in a new pathway of vesicle formation: First, stable droplets are formed, in our case triggered by spinodal decomposition. Then, copolymers aggregate to these nuclei, and they grow larger and larger. As the droplets grow, they first rearrange internally into micelles and then into semivesicles. Finally, solvent is absorbed into the semivesicle and swells the solvent-philic copolymer blocks in the center of the semivesicle. A complete vesicle is built which continues to grow till all copolymers in solution are exhausted. Coalescence events have not been observed. They are presumably prevented kinetically by the solvent-philic corona, which surrounds the micelles and vesicles with a repulsive shell.

The two pathways of vesicle formation can probably coexist in certain systems, depending on the copolymer concentration, the chain length, and the interaction parameters. For long and weakly interacting amphiphilic molecules in dilute solution, the mechanism of nucleation and growth apparently dominates the process of vesicle formation. In this regime, the final vesicle size is basically determined by the initial density of droplets. Nuclei which have been formed early evolve

into large vesicles, whereas nuclei formed later stay small or even become unstable. Thus the vesicle size (in terms of amphiphiles per vesicle) is given by the ratio of the average amphiphile concentration and the droplet density n_s (Fig. 8b), and the scales like the inverse density (data not shown).

This opens a way to tune the nucleation process and to control the vesicle formation. We propose to use a prenucleation method through adding a definite number of small sphere micelles as seeds (The seeding method is also widely used to control crystallization of materials). To test this idea, we have performed simulations starting from special initial states, which contained a definite number of small sphere micelles. Figure 13 shows the resulting vesicle structures. With 12 seeds, smaller vesicles are obtained (Fig. 13a), and with 6 seeds, larger vesicles are formed (Fig. 13b). This preliminary result shows that it is possible to control the size and uniformity of vesicle using a simple seeding method, in systems where the vesicle formation is controlled by nucleation and growth.

To summarize, we have for the first time simulated the dynamic formation of vesicles of amphiphilic diblock copolymers in dilute solution, using the external potential dynamics method developed from the polymer self-consistent mean field theory. Initially homogenous systems were quenched into the unstable part of the two-phase region close to spinodal line. We have discovered a new pathway of spontaneous vesicle formation, which differs from the conventional one: First, spinodal decomposition triggers the nucleation of droplets, then the droplets restructure themselves into sphere micelles, subsequently the sphere micelles transform to semivesicle, and finally, the semivesicles grow into complete vesicle structures. The process of vesicle formation in such a system is controlled by nucleation and growth. The solvent-philic segments play a critical role for the initial stage of nucleation, and for the transformation of semivesicles to vesicles. The size and uniformity of the (metastable) vesicles strongly depends on the number of nuclei and the uniformity of nucleation. A simple method, prenucleation through adding small sphere micelle as seeds, was proposed to control the size of the vesicles.

Acknowledgements.

This research work was financially supported by Alexander von Humboldt foundation through a research fellowship. We thank Dr. Thomas Gruhn for a valuable discussion.

References

1. Petty, H. R. *Molecular Biology of Membranes, Structure and Function*, Plenum: New York, 1993.

2. Zhang, L.; Eisenberg, A. *Science* 1995, *268*, 1728.

3. Zhang, L.; Eisenberg, A. *Macromolecules* 1996, *29*, 8805.

4. Luo, L.; Eisenberg, A. *Langmuir* 2001, *17*, 6804.

5. Gravano, S.; Borden, M. A.; Werne, T. von; Doerffler, E. et al. *Langmuir* 2002, *18*, 1938.

6. Kickelbick, G.; Bauer, J.; Husing, N.; Andersson, M.; Palmqvist, A. *Langmuir* 2003, *19*, 3198.

7. Discher, D. E.; Eisenberg, A. *Science*, 2002, *297*, 967.

8. Discher, B. M.; Won Y.-Y.; Ege, D. S.; Lee, J. C.-M.; Bates, F. S.; Discher, D. E.; Hammer, D. A. *Science* 2001, *284*, 1143.

9. Antonietti, M.; Forster, S. *Adv. Mater.* 2003, *15*, 1323.

10. Seifert U.; Lipowsky, R. *In Structure and Dynamics of Membranes*; Lipowsky, R.; Sackmann, E., Ed.; Elsevier Science BV: Amsterdam, 1995.

11. Helfrich, W. *Z Naturforsch., Teil A* 1973, *28*, 693.

12. Safran, S. A.; Pincus, P.; Andelman, D. *Science* 1990, *248*, 354.

13. Kaler, E. W.; Murthy, A. K.; Rodriguez, B. E.; et al. *Science* 1989, *245*, 1371.

14. Yan, Y.; Xiong, W.; Huang. J. B.; et al. *J. Phys. Chem.* B 2005, *109*, 357.

15. Egelhaaf, S. U.; Schurtenberger, P. *Phys. Rev. Lett.* 1999, *82*, 2804.

16. Weiss, T. M.; Narayanan, T.; Wolf, C.; Gradzielski, M.; Panine, P.; Finet, S.; Helsby, W. I. *Phys. Rev. Lett.* 2005, *94*, 038303.

17 Schmölzer, S.; Gräbner, D.; Gradzielski, M.; Narayanan, T. *Phys. Rev. Lett.* 2002, *88*, 258301.

18. Nieh, M. –P.; Raghunathan, V. A.; et al. *Langmuir* 2005, *21,* 6656.

19. Noguchi, H.; Takasu, M. *Phys. Re*v. *E* 2001, *64*, 041913.

20. Noguchi, H.; Takasu, M. *J. Chem. Phys.* 2001, *115*, 9547.

21. Bernardes, A. T. *J. Phys. II* 1996, *6*, 169-174.

22. Bernardes, A. T. *Langmuir* 1996, *12*, 5763-5767.

23. Yamamoto, S.; Maruyama, Y.; Hyodo, S.-A. *J. Chem. Phys.* 2002, *116*, 5842-5849.

24. de Vries, Al. H.; Mark, A. E.; Marrink, S. J. *J. Am. Chem. Soc.* 2004, *126*, 4488.

25. He, X. H.; Liang, H. J.; Huang, L.; Pan, C. Y. *J. Phys. Chem. B* 2004, *108,* 1731.

26. Schmid, F. *J. Phys. Cond. Matt.* 1998, *10*, 8105.

27. Edwards, S. F. *Proc. Phys. Soc.* 1965, *85*, 613.

28. Helfand, E. *J. Chem. Phys. 1975*, *62*, 999.

29. Matsen, M. W.; Schick, M. *Phys. Re*v. *Lett.* 1994, *72*, 2660.

30. Noolandi, J.; Shi, A.-C.; Linse, P. *Macromolecules* 1996, *29*, 5907.

31. Bohbot-Raviv, Y.; Wang, Z. G. *Phys. Re*v. *Lett.* 2000, *85*, 3428.

32. Drolet, F.; Fredrickson, G. H. *Phys. Rev. Lett.* 1999, *83*, 4317.

33. Drolet, F.; Fredrickson, G. H. *Macromolecules* 2001, *34*, 5317.

34. Fredrickson, G. H.; Ganesan, V.; Drolet, F. *Macromolecules* 2002, *35*, 16.

35. Uneyama, T.; Doi, M. *Macromolecules* 2005, *38,* 5817.

36. Sevink, G. J. A.; Zvelindovsky, A. V. *Macromolecules* 2005, *38,* 7502.

37. Maurits, N. M.; Fraaije, J. G. E. M. *J. Chem. Phys.* 1997, *107*, 5879.

38. Kawasaki, K.; Sekimoto, K. *Physica* 1988, *148A*, 361.

39. Reister, E.; Müller, M.; Binder, K. *Phys. Rev. E* 2001, *64*, 041804.

40. Reister, E.; Müller, M. *J. Chem. Phys.* 2003, *118*, 8476.

41. Müller, M; Schmid, F. in *Advanced Computer Simulation Approaches for Soft Matter Sciences II*, C. Holm and K. Kremer Eds., *Advances in Polymer Science 185*, pp. 1-85 (Springer Verlag, Berlin, 2005).

42. Tzeremes, G.; Rasmussen, K. O.; Lookman, T.; Saxena, A. *Phys. Rev. E.* 2002, *65*, 041806.

43. Frigo, M.; Johnson, S. G. *The Fastest Fourier Transform in the West 2.1.3*; MIT: Cambridge, MA, 2000. (software package freely downloadable from http://www.fftw.org).

44. Cahn, J. W; Hilliard, J. E. J. *Chem. Phys.* 1958, *28*, 258; *ibid* 1959, *31*,688.

45. Langer, J. S.; Bar-on, M.; Miller, H. D. *Phys. Rev. A* 1975, *11*, 1417.

46. Binder K. *Rep. Prog. Phys.* 1987, *50*, 783.

47. Rappl, T. J.; Balsara, N. P. *J. Chem. Phys.* 2005, *122*, 214903.

48. Schmid, F.; Blossey, R. *J. Physique II France* 1994, *4*, 1195.

49. de Gennes, P.-G. *Scaling Concepts in Polymer Physics* (Cornell Univ. Press, London, 1979).

50. Lifshitz, I.M.; Slyozov, V.V *J. Phys. Chem. Solids* 1961, *19*, 35.

51. Wagner, C. *Z. Elektrochemie* 1961, 65, 581.

52. Sagui, C.; Grant, M. *Phys. Rev. E.* 1999, *59*, 4175.

Figure Captions

Fig. 1 Homogeneous mean-field phase diagram for a mixture of amphiphilic diblock copolymers and solvent. The parameters are N=17, c_B=0.118, $\chi_{AS}=1.2$, $\chi_{AB}=1.05$. The spinodal curve was calculated using Eq. (12). The triangles correspond to simulation parameters, i.e., χ_{BS} varied from -0.15 to 0.75.

Fig. 2 Aggregation morphology of amphiphilic diblock copolymers in dilute solution in 2D at various times *t*. Grey, black, and white correspond to A-rich, B-rich and S-rich regions, respectively. The Flory-Huggins parameters are $\chi_{BS}=0.0375$, $\chi_{AS}=1.2$, and $\chi_{AB}=1.05$.

Fig. 3 Aggregation morphology of amphiphilic diblock copolymer in dilute solution in 3D at various times *t*. Only the density distribution of phase A is shown. The Flory-Huggins parameters are $\chi_{BS}=0.0375, \chi_{AS}=1.2, \chi_{AB}=1.05$. The morphology at $t=4.5\times10^5$ corresponds to a semivesicle structure.

Fig. 4 Aggregation morphology of the copolymers at the initial stage ($t\le1.9\times10^5$) using high grey contrast. Black corresponds to copolymer-rich regions.

Fig. 5 Time evolution of the structure factor $S(q,t)$ for early times in 2D. The arrow S marks a peak corresponding to the solvent inside the vesicle. The Flory-Huggins interaction parameters are $\chi_{BS}=0.0375, \chi_{AS}=1.2, \chi_{AB}=1.05$

Fig. 6 Time evolution of the order parameter, $\sigma=\int_V dr\left|\phi_A+\phi_B-f_P\right|/V$ in 2D.

Fig. 7 Aggregation morphology of amphiphilic diblock copolymers in dilute solution in 3D at various times. Only the density distribution of A is shown. The Flory-Huggins

parameters are $\chi_{\mathrm{BS}}=-0.45, \chi_{\mathrm{AS}}=1.2, \chi_{\mathrm{AB}}=1.05$ The morphology at $t=1.21\times10^{6}$ corresponds to a semivesicle structure.

Fig. 8 Density of droplets n_s (a), and starting time for nucleation τ (b) in 2D, as a function of the interaction parameter χ_{BS}. The fitting curves obey the scaling relations $\tau \sim (\chi_{\mathrm{BS}}-\chi_{spinodal})^{\alpha}$, with $\chi_{spinodal}=-0.85$ and $\alpha=1.19\pm0.1$ for n_s (a) and $\alpha=-1.27\pm0.1$ for τ (b).

Fig. 9 Density profiles on a cross section of the cluster marked with the arrow in Fig. 2.

Fig. 10 Aggregation morphology of amphiphilic diblock copolymers in dilute solution after 2.5×10^{6} time steps in 2D. a) $\chi_{\mathrm{BS}}=-0.15, \chi_{\mathrm{AS}}=1.2, \chi_{\mathrm{AB}}=1.05$; b) $\chi_{\mathrm{BS}}=0.375, \chi_{\mathrm{AS}}=1.2, \chi_{\mathrm{AB}}=1.05$; c) $\chi_{\mathrm{BS}}=0.6, \chi_{\mathrm{AS}}=1.2, \chi_{\mathrm{AB}}=1.05$

Fig. 11 Examples of Ostwald-like ripening. (a,b) show morphologies for $\chi_{\mathrm{BS}}=-0.15$ at 6.0×10^{5} time steps (a) and 2.3×10^{6} time steps (b). A semivesicle marked with O shrinks into a sphere micelle; (c,d) show morphologies for $\chi_{\mathrm{BS}}=0.75$ at 7.0×10^{5} time steps (c) and 2.95×10^{6} time steps (d). Two sphere micelles marked with U disappear.

Fig. 12 Dependence of the free energy *F*, the energies $E_{\mathrm{A}}, E_{\mathrm{B}}, E_{\mathrm{S}}$ and the entropies $SS_{\mathrm{P}}, SS_{\mathrm{S}}, SS_{\mathrm{P+S}}$ on the time for the case of $\chi_{\mathrm{BS}}=0.0375, \chi_{\mathrm{AS}}=1.2, \chi_{\mathrm{AB}}=1.05$ in 2D. The curves of SS_{P}, SS_{S} and $SS_{\mathrm{P+S}}$ were shifted by a constant.

Fig. 13 Vesicles formed from initial states with various number of small sphere micelles as seeds ($t=5.3\times10^{6}$). a) 12 seeds; b) 6 seeds.

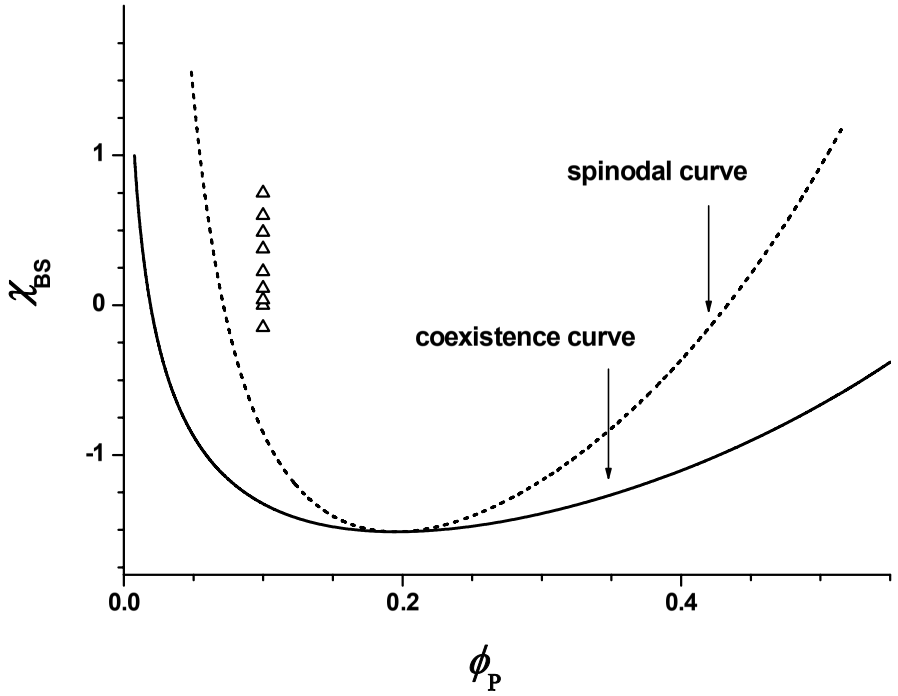

Fig. 1

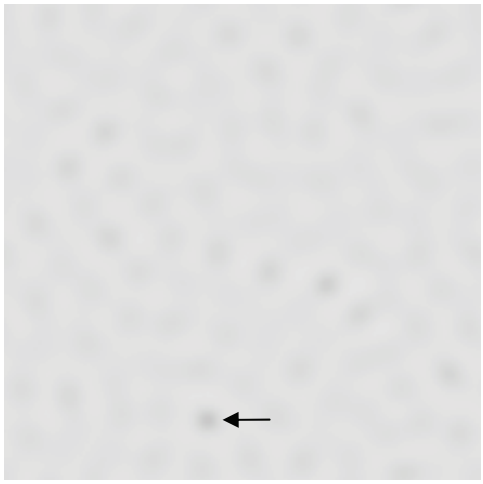

$t = 3.3 \times 10^5$

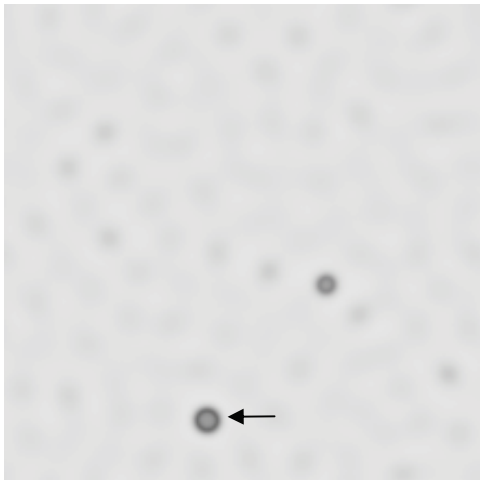

$t = 3.4 \times 10^5$

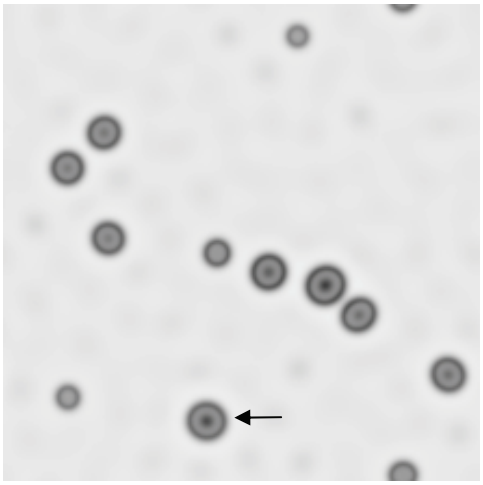

$t = 3.6 \times 10^5$

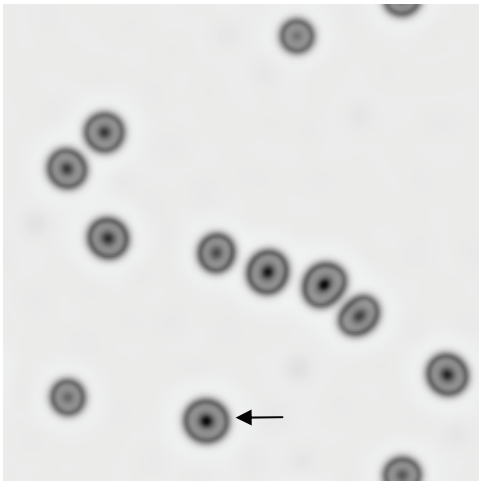

$t = 4.0 \times 10^5$

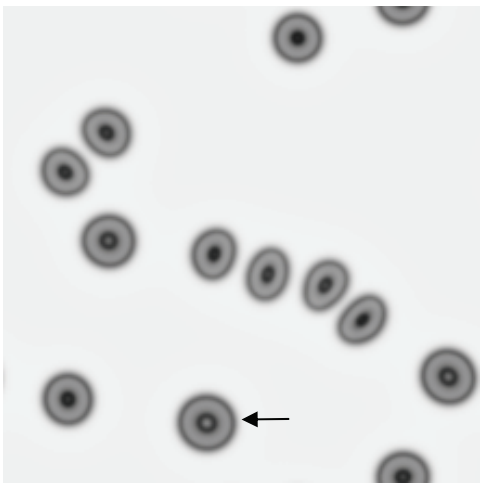

$t = 5.0 \times 10^5$

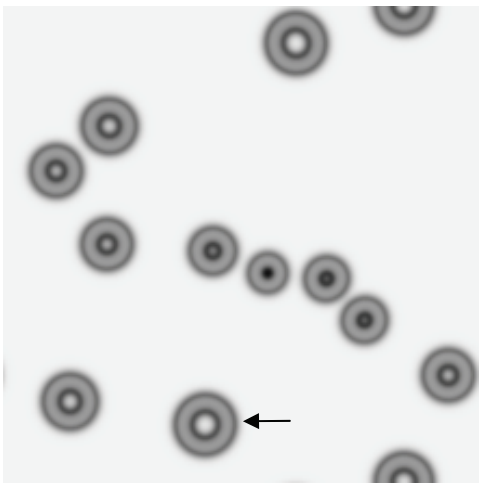

$t = 2.9 \times 10^6$

Fig. 2

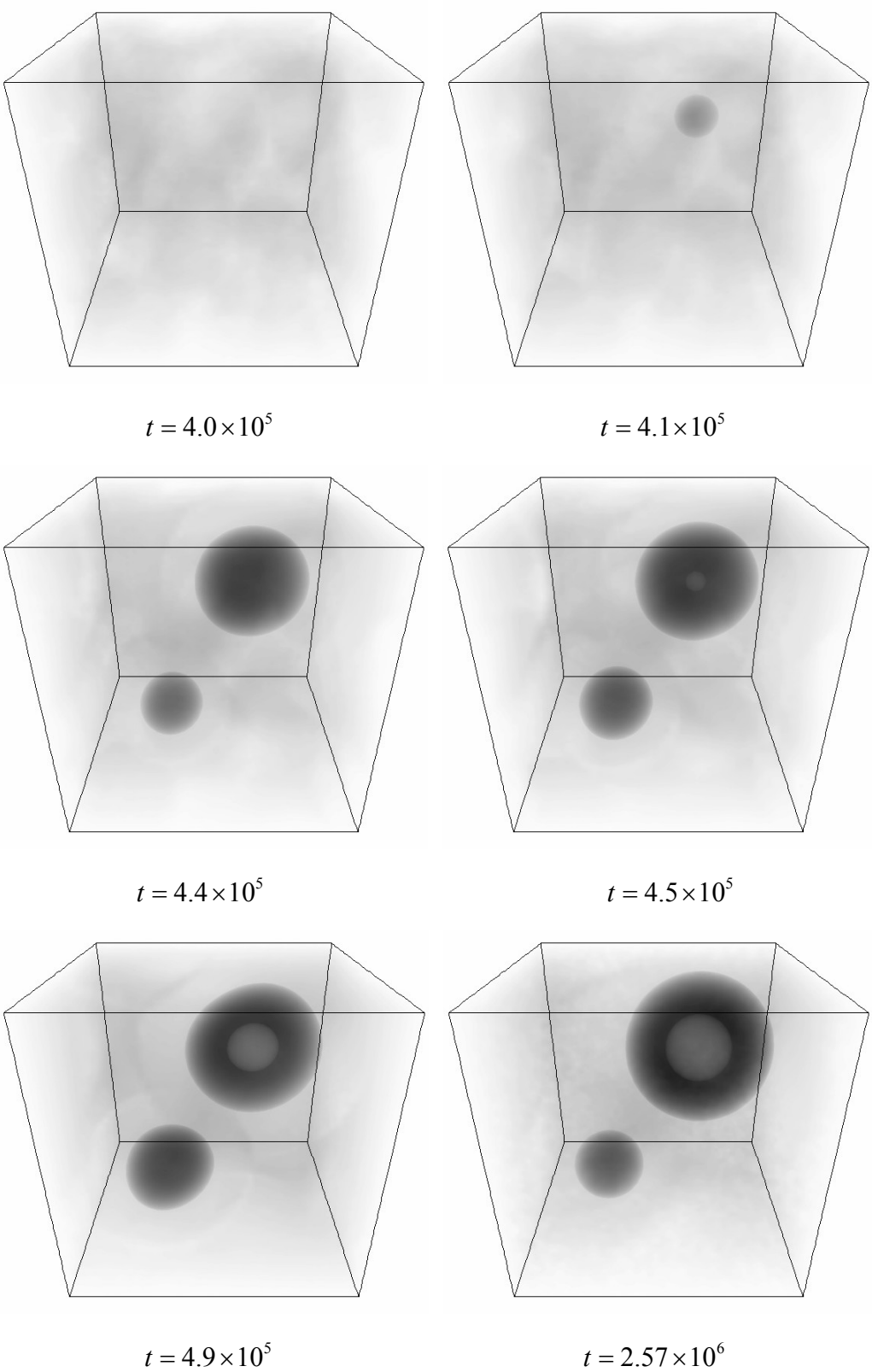
$t = 4.0 \times 10^5$
$t = 4.1 \times 10^5$
$t = 4.4 \times 10^5$
$t = 4.5 \times 10^5$
$t = 4.9 \times 10^5$
$t = 2.57 \times 10^6$

Fig. 3

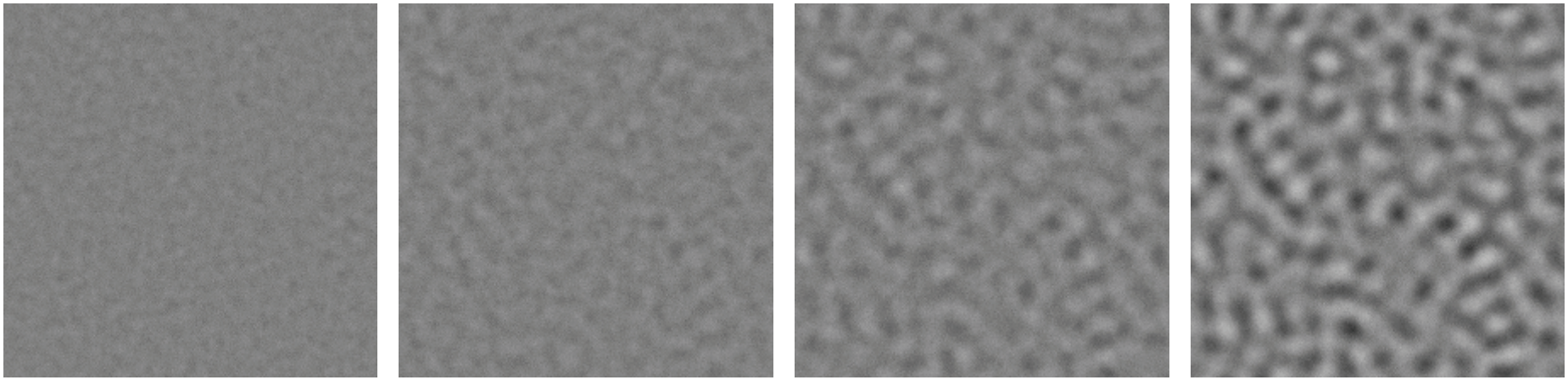

Fig. 4

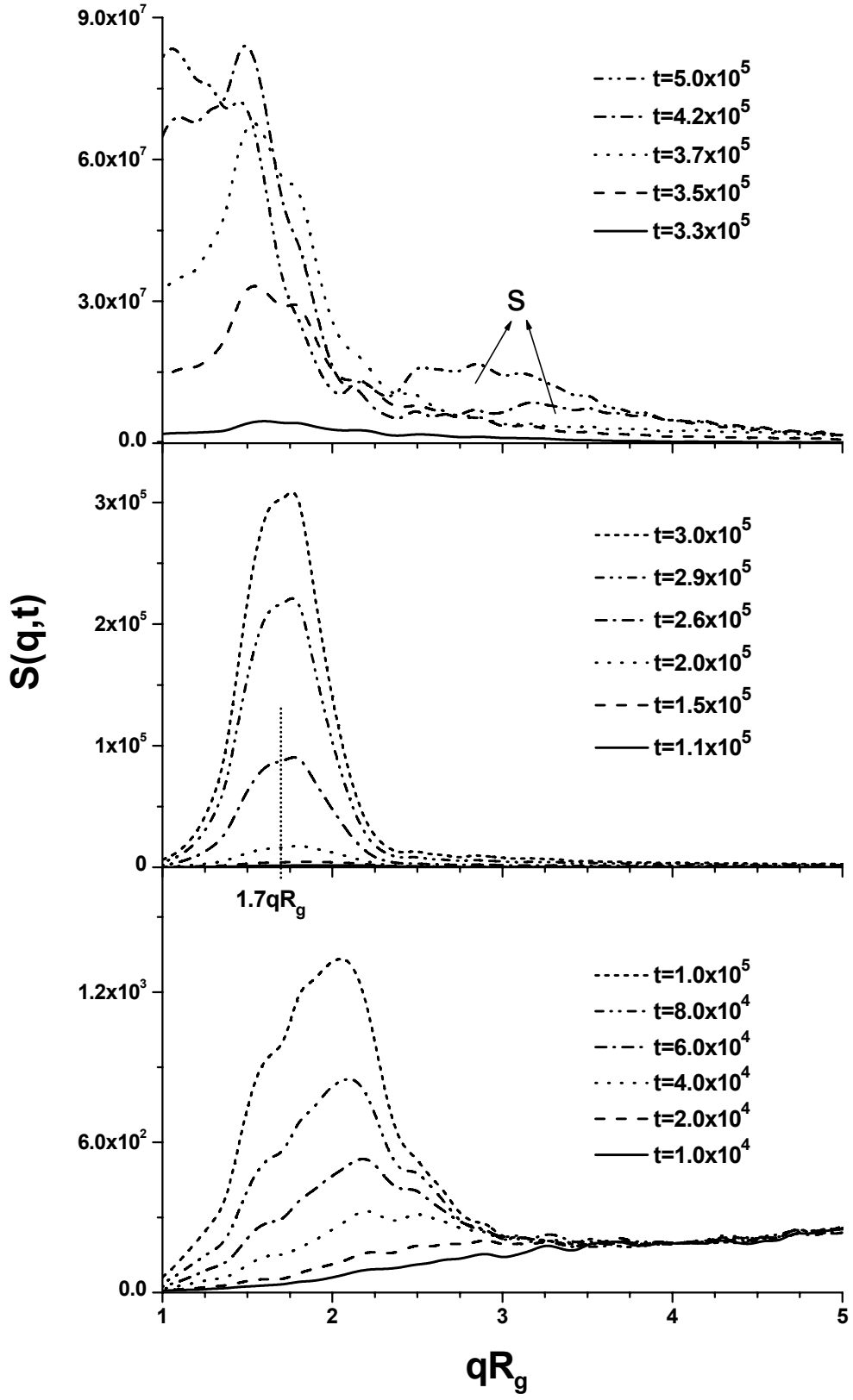
9.0x10^7
6.0x10^7
3.0x10^7
0.0
t=5.0x10^5
t=4.2x10^5
t=3.7x10^5
t=3.5x10^5
t=3.3x10^5
S
3x10^5
2x10^5
1x10^5
0
t=3.0x10^5
t=2.9x10^5
t=2.6x10^5
t=2.0x10^5
t=1.5x10^5
t=1.1x10^5
1.7qR_g
1.2x10^3
6.0x10^2
0.0
t=1.0x10^5
t=8.0x10^4
t=6.0x10^4
t=4.0x10^4
t=2.0x10^4
t=1.0x10^4
1
2
3
4
5
S(q,t)
qR_g

Fig. 5

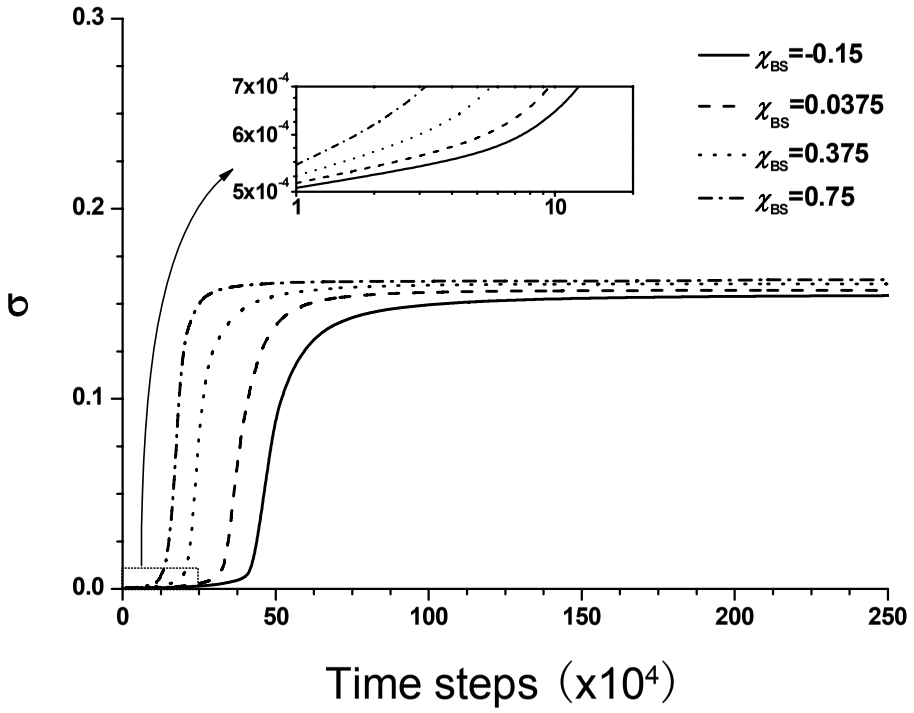
0.3
0.2
0.1
0.0
Q
0
50
100
150
200
250
Time steps（x10⁴）
7x10⁻⁴
6x10⁻⁴
5x10⁻⁴
1
10
χBS=-0.15
χBS=0.0375
χBS=0.375
χBS=0.75

Fig. 6

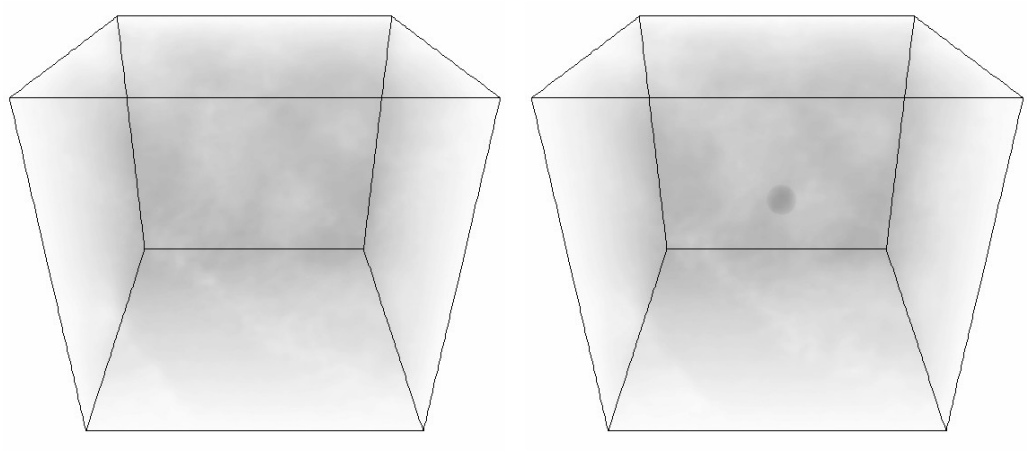

$t = 1.16 \times 10^6$ $t = 1.17 \times 10^6$

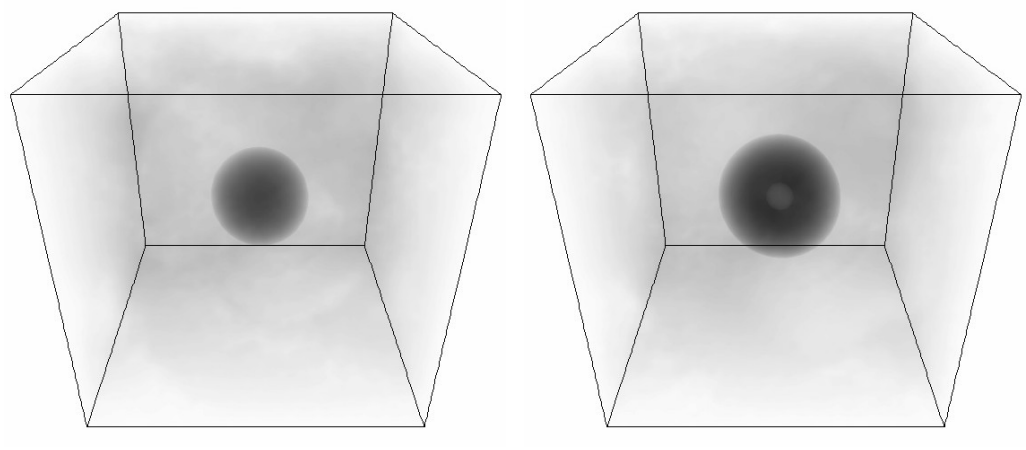

$t = 1.19 \times 10^6$ $t = 1.21 \times 10^6$

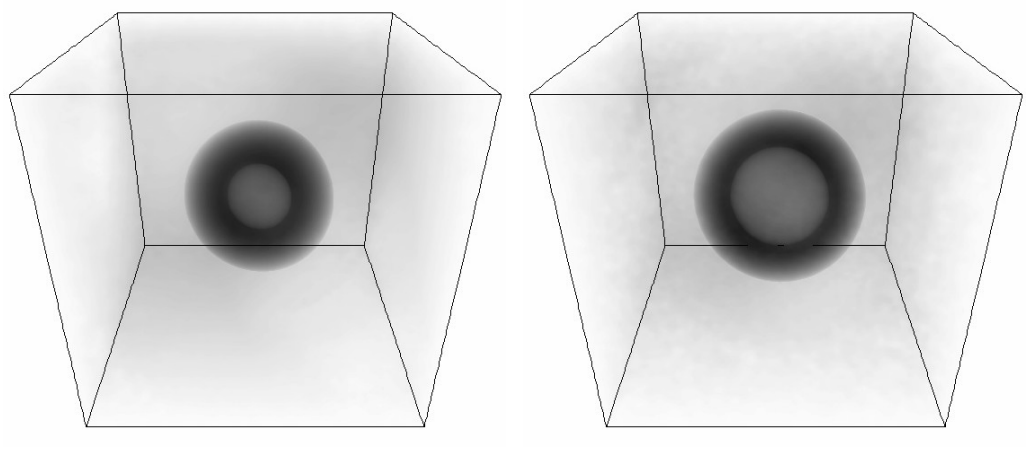

$t = 1.25 \times 10^6$ $t = 1.95 \times 10^6$

Fig. 7

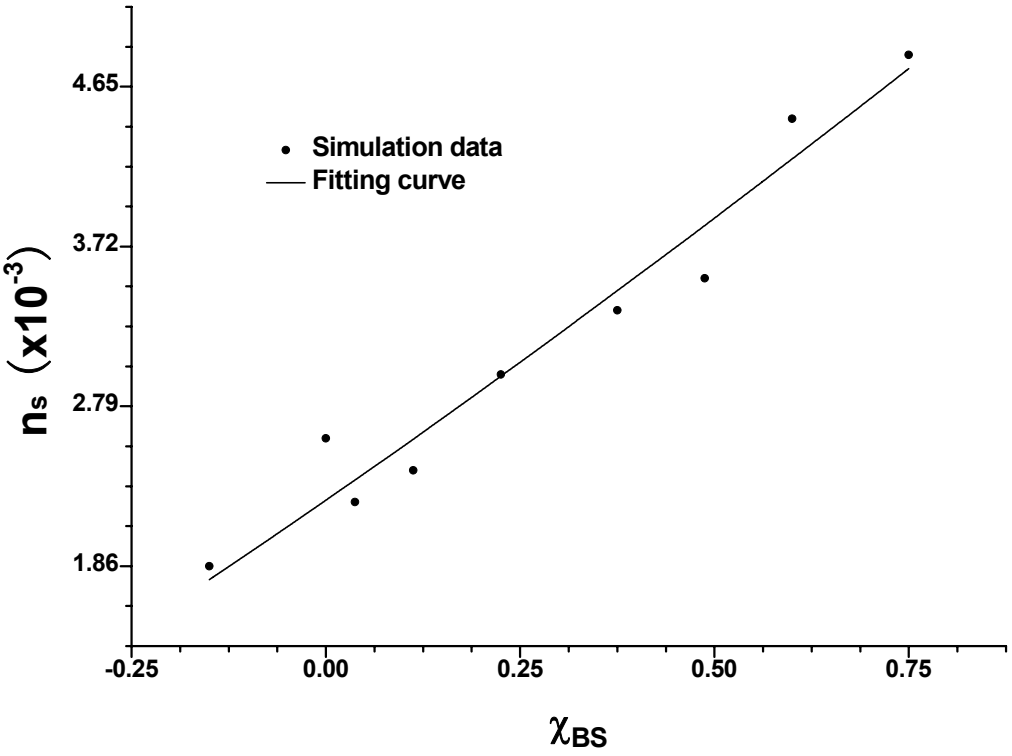
4.65
3.72
2.79
1.86
n_s ($x10^{-3}$)
Simulation data
Fitting curve
-0.25
0.00
0.25
0.50
0.75
χ_{BS}

Fig. 8a

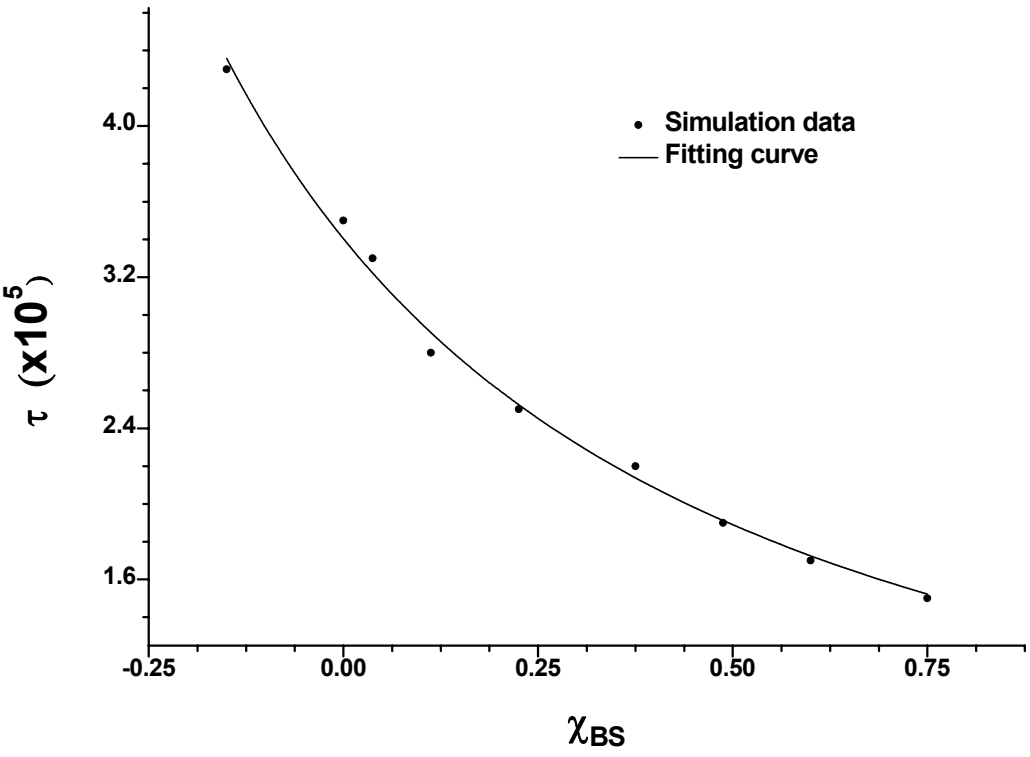
Simulation data
Fitting curve
4.0
3.2
2.4
1.6
τ (x10^5)
-0.25
0.00
0.25
0.50
0.75
χBS

Fig. 8b

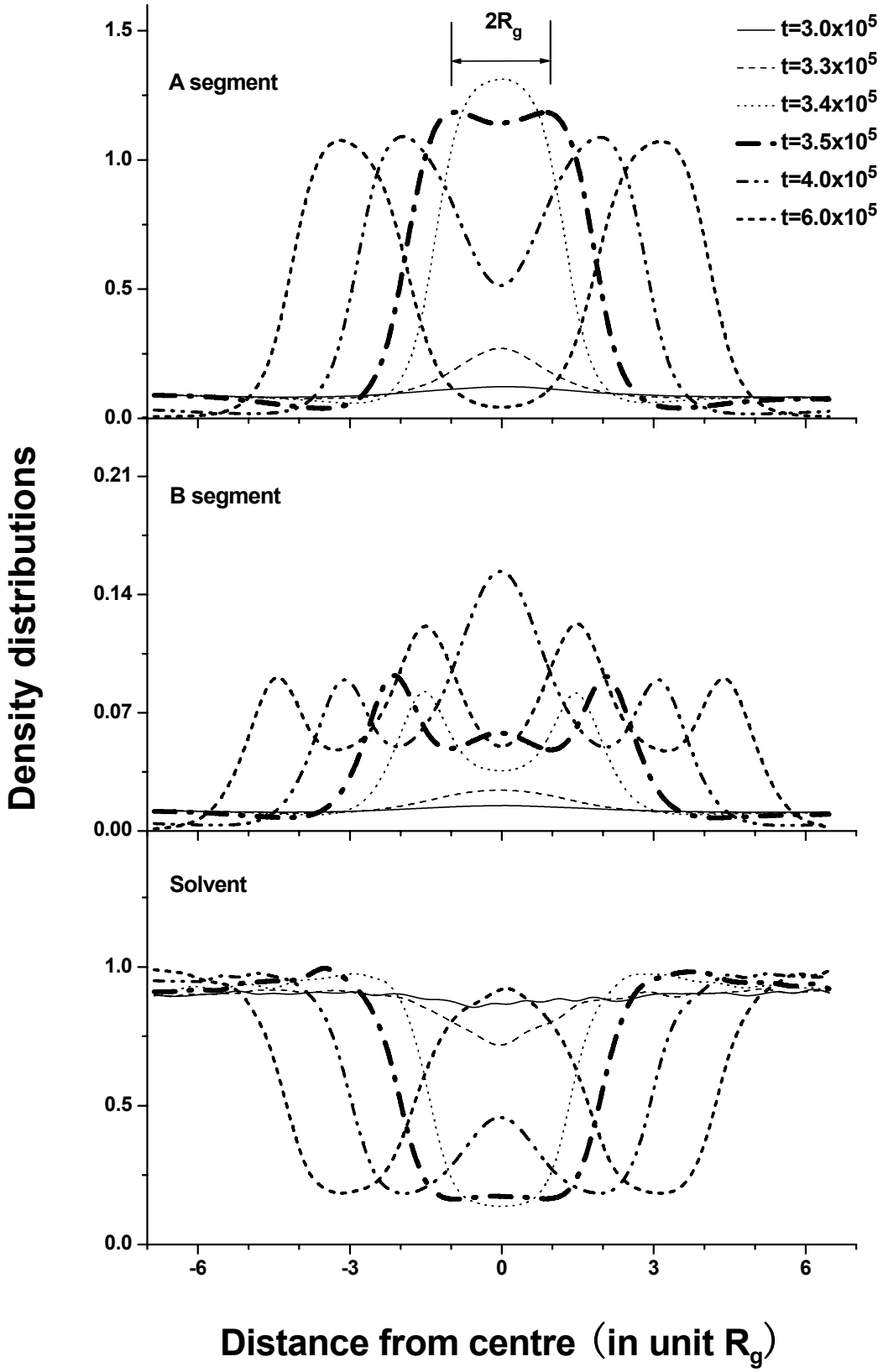
2Rg
t=3.0x10^5
t=3.3x10^5
t=3.4x10^5
t=3.5x10^5
t=4.0x10^5
t=6.0x10^5
A segment
B segment
Solvent
Density distributions
Distance from centre（in unit Rg）
1.5
1.0
0.5
0.0
0.21
0.14
0.07
0.00
-6
-3
0
3
6

Fig.9

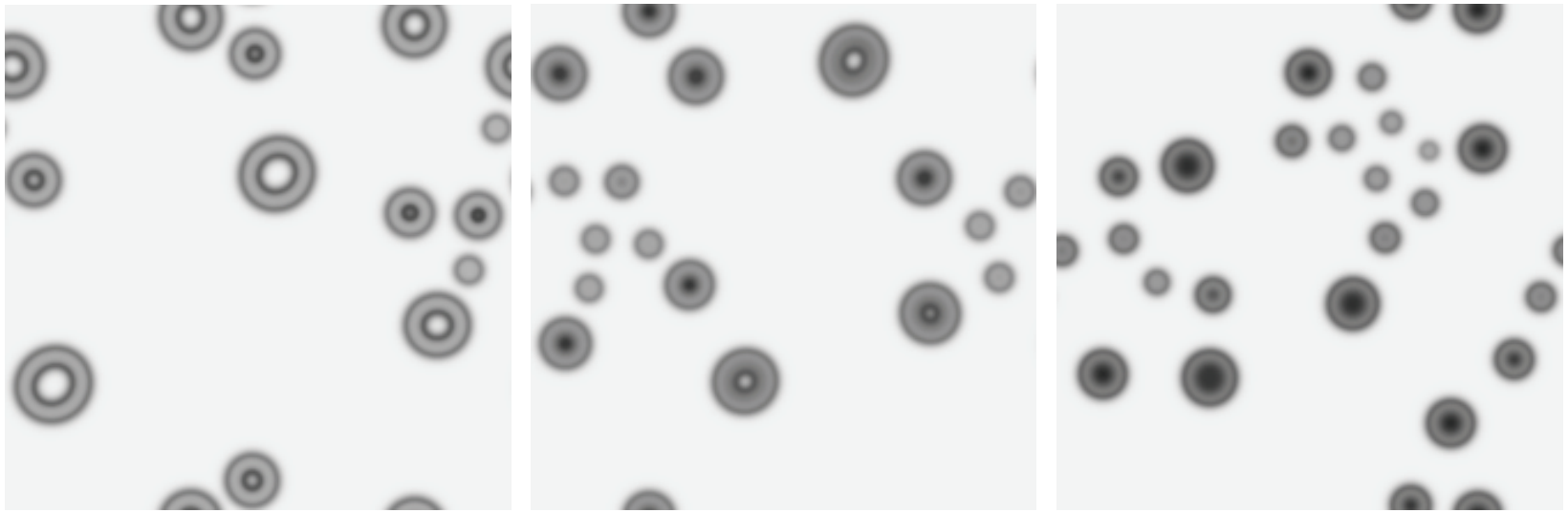

a **b** **c**

Fig. 10

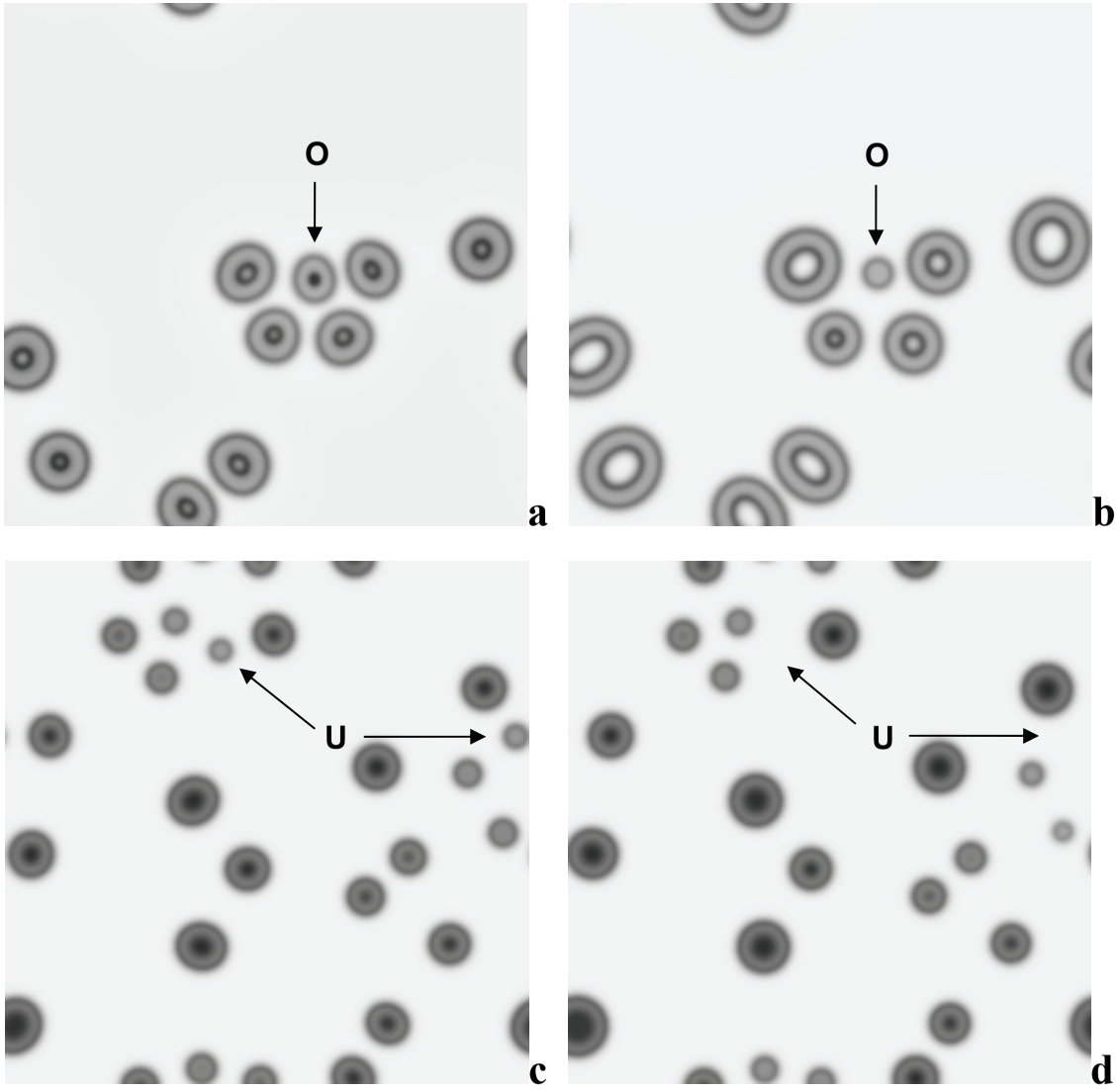

Fig. 11

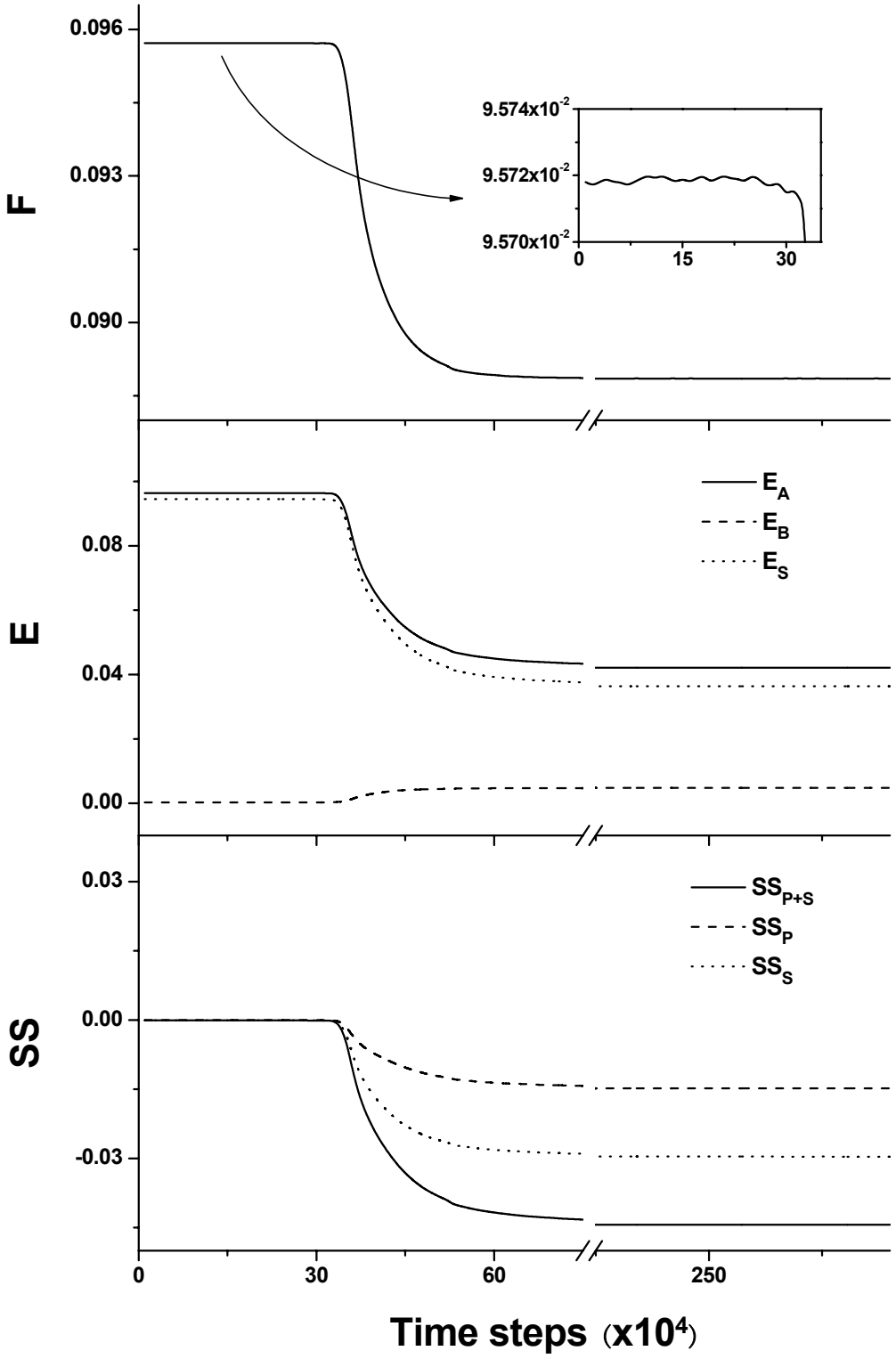
F
0.096
0.093
0.090
9.574x10-2
9.572x10-2
9.570x10-2
0
15
30
E
0.08
0.04
0.00
EA
EB
ES
SS
0.03
0.00
-0.03
SSP+S
SSP
SSS
0
30
60
250
Time steps (x10⁴)

Fig. 12

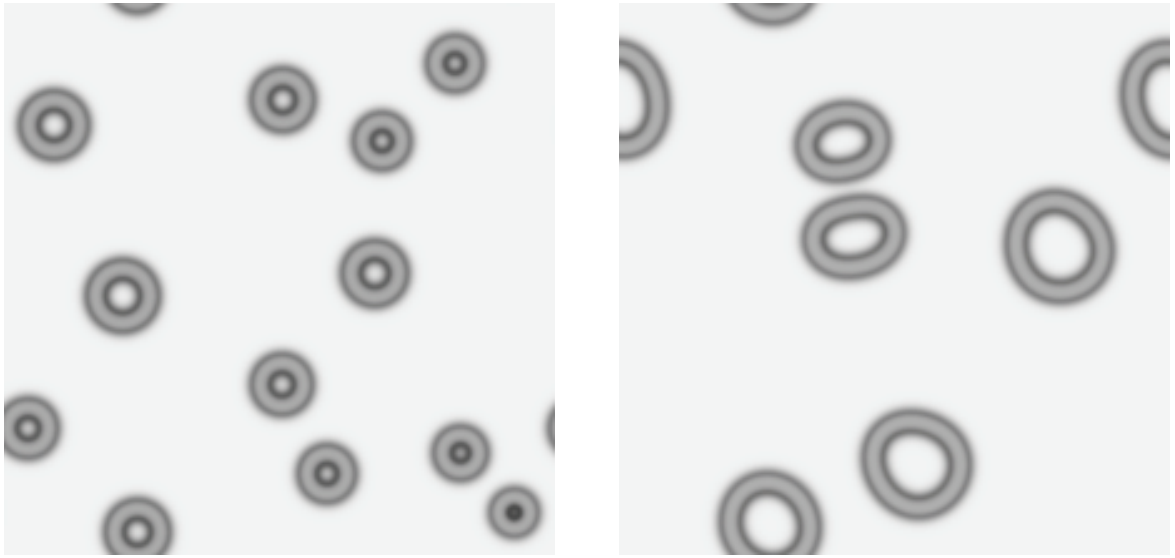

a **b**

Fig. 13

For Table of Contents Use Only

Dynamics of Spontaneous Vesicle Formation in Dilute Solutions of Amphiphilic Diblock Copolymers

X. H. He and F. Schmid